AGU PUBLICATIONS

JGR

Journal of Geophysical Research: Oceans

RESEARCH ARTICLE

10.1002/2016JC011779

Special Section:
Atmosphere–Ice–Ocean–Ecosystem Processes in a Thinner Arctic Sea Ice Regime: The Norwegian Young Sea ICE Cruise 2015 (N–ICE2015)

Vertical fluxes of nitrate in the seasonal nitracline of the Atlantic sector of the Arctic Ocean

Achim Randelhoff[1,2], Ilker Fer[3], Arild Sundfjord[2], Jean-Éric Tremblay[4], and Marit Reigstad[1]

[1]Institute for Arctic and Marine Biology, UiT The Arctic University of Norway, Tromsø, Norway, [2]Norwegian Polar Institute, Tromsø, Norway, [3]Geophysical Institute, University of Bergen and Bjerknes Centre for Climate Research, Bergen, Norway, [4]Québec-Océan and Takuvik, Département de biologie, Université Laval, Québec, Canada

Abstract This study compiles colocated oceanic observations of high-resolution vertical profiles of nitrate concentration and turbulent microstructure around the Svalbard shelf slope, covering both the permanently ice-free Fram Strait and the pack ice north of Svalbard. The authors present an overview over the seasonal evolution of the distribution of nitrate and its relation to upper ocean stratification. The average upward turbulent diffusive nitrate flux across the seasonal nitracline during the Arctic summer season is derived, with average values of 0.3 and 0.7 mmol m^{-2} d^{-1} for stations with and without ice cover, respectively. The increase under ice-free conditions is attributed to different patterns of stratification under sea ice versus open water. The nitrate flux obtained from microstructure measurements lacked a seasonal signal. However, bottle incubations indicate that August nitrate uptake was reduced by more than an order of magnitude relative to the May values. It remains inconclusive whether the new production was limited by an unidentified factor other than NO_3^- supply in late summer, or the uptake was underestimated by the incubation method.

Key Points:
- The nitrate drawdown in the photic zone is empirically strongly related to the development of seasonal stratification from ice melt
- Upward turbulent nitrate fluxes across the seasonal nitracline are small compared to estimates of annual nitrate drawdown on the shelves
- Under a future seasonal Arctic ice cover, increases in seasonal nitrate fluxes can be significant in the deep Eurasian Basin

Correspondence to:
A. Randelhoff,
achim@npolar.no

Citation:
Randelhoff, A., I. Fer, A. Sundfjord, J.–É. Tremblay, and M. Reigstad (2016), Vertical fluxes of nitrate in the seasonal nitracline of the Atlantic sector of the Arctic Ocean, *J. Geophys. Res. Oceans*, *121*, 5282–5295, doi:10.1002/2016JC011779.

Received 7 MAR 2016
Accepted 20 JUN 2016
Accepted article online 23 JUN 2016
Published online 31 JUL 2016

1. Introduction

The paradigm of upper ocean primary productivity divides the production into "new" (based on allochthonous nitrogen, N, mostly nitrate, NO_3^-) and "regenerated" (autochthonous N, mostly ammonium, NH_4^+) production, and defines an f-ratio as the ratio of new production to total (i.e., sum of new and regenerated) production [e.g., *Dugdale and Goering*, 1967]. In this picture, once the phytoplankton bloom has consumed all available nitrate (high f-ratio), vertical fluxes across the base of the mixed layer are the only source of additional allochthonous nitrate, thereby constraining new (i.e., nitrate-based) production locally, leading to a small f-ratio in a community that feeds mostly on recycled nutrients. Strong seasonality of both photosynthetically available radiation and stratification in the upper Arctic Ocean leads to a seasonal cycle in nutrient concentrations, where nutrients are consumed during summer and replenished during winter. Apart from systems where (e.g., coastal) upwelling can lead to pulsed input of nutrients and intermittent or even sustained blooming [e.g., *Tremblay et al.*, 2011], the major mode of nutrient supply to a postbloom ocean surface is diapycnal turbulent diffusion.

The significance of this vertical turbulent flux is twofold: on one hand, it contributes to the depth-integrated drawdown of nitrate. This can act as a measure of net community production, and thus also maximum possible vertical export of carbon [*Tremblay et al.*, 2015]. When averaging over horizontal scales large enough to neglect advection with ocean currents, the vertical diffusive flux must also balance export production (i.e., N that is exported to "depth") on interannual time scales [*Eppley and Peterson*, 1979] (plus harvest of marine resources, if the system is not closed). On smaller scales, however, advection can significantly impact nutrient budgets as on the in and outflow shelves of the Arctic Ocean [*Torres-Valdés et al.*, 2013].

On the other hand, even if the effect of the vertical nitrate flux on the annual nitrate drawdown is small, it determines the availability of NO_3^- versus NH_4^+ and therefore potentially ecosystem composition (favoring organisms that compete either better or worse for nitrate).

In qualitative terms, the nitrate flux (F_N) is often assumed to be small due to the strong stratification in the seasonal pycnocline, but its magnitude and the processes behind remain to be quantified. In addition, upper ocean stratification in the Arctic might change as a consequence of increasing sea ice melt rates [e.g.,

Stroeve et al., 2011], leading to additional uncertainties about future nutrient supply. Few observations of the upward turbulent nitrate flux in the Arctic exist as of now, often biased either toward a season, local processes, or by undersampling, and are thus potentially not representative of average figures. Here, we present average diffusive nitrate fluxes across the Arctic summer nitracline in ice-covered and open water conditions by compiling ocean microstructure and nitrate concentration profiles from the pack ice north of Svalbard, the Svalbard shelf slope and Fram Strait. The wider area around Svalbard is a region of strong horizontal gradients, featuring both perennial and seasonal ice cover and stratification, and the boundary current inflow of warm Atlantic Water (AW) along the shelf slope. In this study, we aim to quantify postbloom $F_{\mathcal{N}}$ across this wide range of conditions common to the Arctic Ocean and elucidate its relation to NO_3^- -based production.

2. Methods

2.1. Data

Colocated continuous vertical profiles of nitrate concentrations ($\mathcal{N}$) and turbulent microstructure were collected during four campaigns spanning the shelf, shelf slope area, Fram Strait and Nansen Basin west and north of Svalbard (Figure 1), and various types of ice cover, from open water and broken-up floes at the ice edge to near-complete ice cover.

Three of the campaigns were conducted in January, May, and August 2014, as part of the CarbonBridge project, aboard the ice-reinforced R/V Helmer Hanssen. Profiles were collected both on cross-shelf slope transects and on dedicated process stations with detailed measurements of biogeochemistry and lower trophic levels, including sampling both in the open water (ship-based) and in the marginal ice zone (either ship-based or from nearby ice floes). Microstructure shear was measured (only in May and August) using a loosely-tethered microstructure profiler MSS-90L (IWS Wassermesstechnik) with two airfoil shear probes, falling freely at a rate of $\sim$0.55 m s^{-1}. The microstructure shear is needed to obtain the vertical eddy diffusivity, K_ρ, used in calculation of nutrient fluxes (section 2.5). The microstructure sampling was made in sets of at least three consecutive repeat profiles. $\mathcal{N}$ was measured using an unpumped ISUS V3 (Satlantic), mounted on the shipboard SBE911+ (Sea-Bird Electronics, Bellevue, WA, USA) CTD (conductivity-temperature-depth) rosette system logging the analog output voltage of the ISUS. Downcast speed in the upper 200 m was 0.6 m s^{-1} and 1.0 m s^{-1} after that.

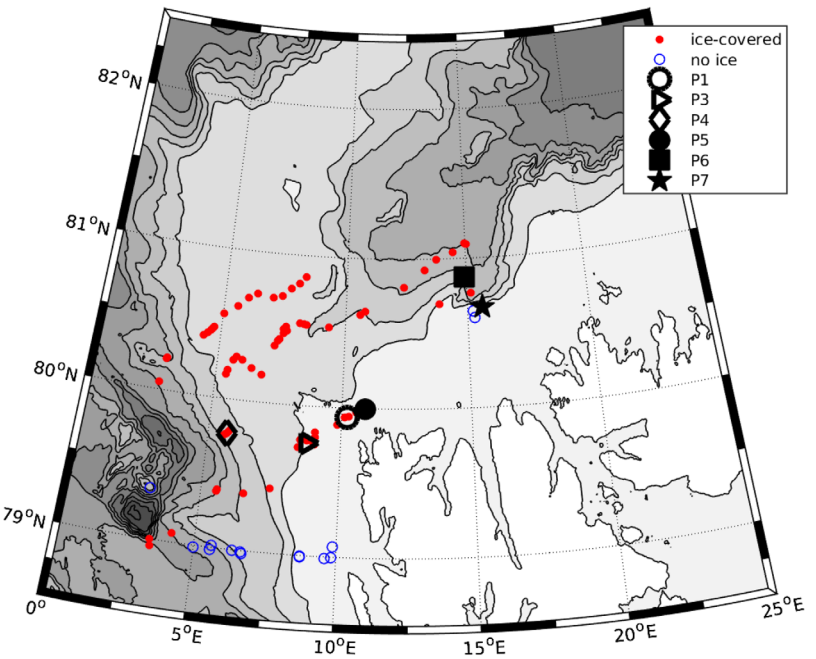

Figure 1. Location of nitrate and microstructure profiles used for $F_{\mathcal{N}}$ estimates. Bottom topography based on IBCAO V3 [*Jakobsson et al.*, 2012] and contoured at 500 m intervals. The white region is the Svalbard Archipelago.

A total of six free-drift process stations of approximately 24 h duration were conducted (location: see Figure 1) with bottle-incubation-based estimates of new and regenerated production in addition to multiple sets of microstructure data and ISUS profiles.

The fourth campaign was the N-ICE drift [*Granskog et al*., 2016], lasting from January to June 2015, based off R/V Lance, which was frozen into the ice or moored to a total of four successive ice floes during the 6 month period (with short breaks for relocation between ice camps). Sampling included at least one set of MSS casts a day (to 200–300 m depth, fall rates $\sim$0.8 m s^{-1}) and biweekly ISUS casts (to 120 m depth), with ISUS deployment frequency increasing to almost daily with the onset of the observed spring bloom in late May. Again, the ISUS was used in an unpumped configuration, mounted on a frame with an SBE19+ system that was programmed to sample the analog output voltage of the ISUS. The downcast speed during the N-ICE campaign was $\sim$0.2 m s^{-1} to meet the requirements of another instrument mounted on the same frame. Both MSS and ISUS were deployed through a hydrohole from a tent several hundred meters away from the ship.

A total of 130 ISUS profiles and 440 MSS casts were collected. In addition, three ISUS profiles across the Yermak plateau collected from R/V Polarstern in June 2015 as part of the TRANSSIZ cruise are presented to supplement the discussion of the large-scale distribution of nitrate.

2.2. Processing of MSS Data

MSS data were processed following *Fer* [2006]. Assuming local small-scale isotropy [*Yamazaki and Osborn*, 1990], dissipation of turbulent kinetic energy was estimated from the measured microscale shear as

$$\epsilon = 7.5\nu\langle(\partial_z u')^2\rangle, \tag{1}$$

where ν is the molecular viscosity of sea water and $\partial_z u'$ the turbulent shear. Resulting dissipation profiles are averaged in bins of 0.5 m. Eddy diffusivity of mass was estimated as $K_\rho = \Gamma\frac{\epsilon}{N^2}$, where the mixing efficiency is taken as $\Gamma = 0.2$ [*Osborn*, 1980] and N is the buoyancy frequency. In this study, for the flux calculations, K_ρ is obtained from the average dissipation over the depth range of the nitracline, and N from the density gradient across the nitracline (see section 2.5).

2.3. Processing of CTD and ISUS Data

CTD data were processed using standard SBE routines. To align the time stamps of ISUS and CTD, raw ISUS output logged on both ISUS and the respective CTD system were compared to find the time lag that produced the maximum correlation, and T and S records were then aligned to ISUS records. The internally logged absorption spectra were then processed mainly following *Sakamoto et al*. [2009], using their "temperature compensated, salinity subtracted" algorithm and a wave band of 217–240 nm. Resulting $\mathcal{N}$ profiles generally have a small (median 0.9 μM) depth-independent offset compared to bottle samples, but capture the vertical gradients well. Because $F_\mathcal{N}$ is obtained from vertical gradients (see section 2.5), the estimates do not depend on how the bias is determined. Details of the quality control and postprocessing procedure are deferred to Appendix A.

2.4. Nutrient Sample Analysis

For quality control and calibration, the ISUS profiles are supplemented with water sample profiles of nitrate concentrations from all campaigns, analyzed with standard methods. For CarbonBridge and TRANSSIZ, bottle samples were frozen until analysis at the University of Tromsø using a Flow Solution IV analyzer from O.I. Analytical, USA, calibrated with reference sea water from Ocean Scientific International Ltd., UK. The N-ICE nutrient samples were fixed with chloroform and stored cool until spectrophotometric analysis at the Institute of Marine Research, Norway, using a modified Skalar autoanalyzer [*Bendschneider and Robinson*, 1952]. $\mathcal{N}$ is significant to one decimal for both analyses, and detection limits are 0.02 μM for CarbonBridge and TRANSSIZ and 0.4 μM for N-ICE.

2.5. Calculation of Nitrate Fluxes

The definition of $F_\mathcal{N}$ employed in this study is $F_\mathcal{N} = K_\rho\frac{\partial\mathcal{N}}{\partial z}$, where the vertical eddy diffusivity of mass K_ρ and the vertical nitrate gradient $\frac{\partial\mathcal{N}}{\partial z}$ (defined positive upward) are both bulk quantities calculated over the nitracline. The nitracline is defined in terms of a density-scaled depth coordinate based on the CTD cast

associated with the ISUS profile in order to eliminate the effect of isopycnal displacements in the calculation of K_ρ. Details are deferred to Appendix B.

All ~130 ISUS profiles collected during the four campaigns are used to present nitrate distribution patterns, covering the period from January 2014 to June 2015. The upward turbulent nitrate flux across the nitracline is quantified using a total of ~440 MSS casts and ~100 ISUS casts, resulting in a total of ~90 viable $F_{\mathcal{N}}$ estimates (i.e., where ISUS profiles contain a nitracline following the definition). Pooling the 2014 and 2015 data, the flux estimates cover the productive period between May and August as they are restricted to situations where the surface layer has experienced significant nitrate drawdown.

2.6. Primary Production Incubations

Water samples for incubations were taken at 0, 5, 10, 20, 30, 40, 50, and 75 m and subdivided in four 500 mL polycarbonate bottles for each depth. Two of the bottles were spiked with 15*N* ammonium chloride and two were spiked with 15*N* potassium nitrate, using the minimum amount of tracer (0.1 μM) required to get a reliable labeling signal. The bottles were hooked on a surface-tethered mooring and incubated in situ for 24 h. Incubations were terminated by filtration onto 24 mm glass microfiber filters (Whatman GF/F; vacuum pressure $<$250 mm Hg). All filters were desiccated at 60°C and stored dry for postcruise analysis. An elemental analyzer (ECS 4010, Costech Analytical Technologies Inc.) coupled to a mass spectrometer (Delta V Advantage, ThermoFinnigan) was used to determine isotopic enrichment and particulate organic carbon and nitrogen using a modified Dumas method (for details see *Blais et al*. [2012]). Nitrogen uptake was calculated using equation (3) of *Collos* [1987]:

$$\text{N uptake} = \left[N_f \cdot (C_p - C_0)\right] / \left[(C_d - C_0)\Delta t\right] \quad (2)$$

where N_f is the concentration of particulate organic nitrogen (μg L^{-1}), C_0 and C_p are the atom-% enrichments of the particulate material before and after the incubation, respectively, C_d is the natural 15*N* abundance (atom-%) of dissolved inorganic nitrogen at the beginning of the incubation and Δt is the duration of the incubation (h).

Ammonium concentrations were measured manually with the sensitive fluorometric method [*Holmes et al*., 1999] in order to supplement the discussion of the incubation results. Reagents were added within minutes of sample collection.

3. Results

3.1. Patterns of Upper Ocean Nitrate Distribution

Three contrasting regimes of upper ocean stratification were observed: (1) on-shelf and over the shelf slope where warm and salty AW reached up to the ice-free surface and stratification was weak, (2) late spring and summer, off-shelf and in ice-covered regions, where ice melt had led to haline stratification, and (3) winter, early spring, and deep into the pack ice/deep Arctic basin, where the surface mixed layer extended to 50–100 m depth (Figures 2–4; also note the mixed layer depths). Nitrate drawdown or even depletion was evident wherever there was significant upper ocean stratification (as signified by the density difference between surface and deeper layers; see Figure 5). Note that the two easternmost transects in Figure 2 are from different years, and the location of the ice edge and presence of stratified surface waters at the respective times (not shown) correspond well to where the vertical $\mathcal{N}$ gradient starts to appear.

Four representative profiles of hydrography, turbulent microstructure, and chlorophyll fluorescence (Figure 6) highlight both the seasonal evolution of $\mathcal{N}$ and its relation to the stratification. The two May profiles show a near-depletion of nitrate in the upper 20 m, coincident with elevated concentrations of chl-a fluorescence. The two August profiles show total depletion of surface $\mathcal{N}$ (equal zero to within measurement uncertainty) and a deepening of the nitracline which is not reflected in the pycnocline. However, the chl-a fluorescence now indicates the development of a subsurface chlorophyll maximum at the upper end of the nitracline. As opposed to the open-water profiles, the ice-covered profiles do not have a distinct surface mixed layer. Instead, sea ice melt provides a constant freshwater source that prohibits thorough mixing of the surface layer. Note that the dissipation of turbulent kinetic energy rapidly approaches background values at the base of the seasonal pycnocline, such that the August nitraclines are virtually decoupled from the

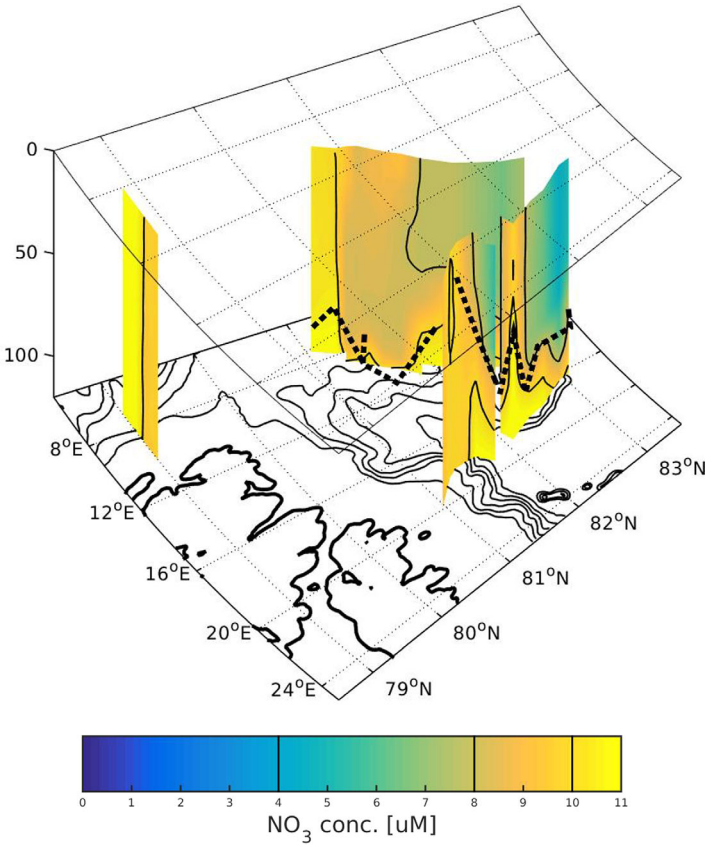

Figure 2. Curtain plots of nitrate concentration $\mathcal{N}$: Winter (N-ICE until 25 May, CarbonBridge January data). Mixed layer depth is plotted into the curtains as dotted lines.

wind-driven surface mixing. A more detailed description of the regional hydrography in relation to biogeochemical parameters will be reported elsewhere.

3.2. Nitrate Fluxes

The population of $F_{\mathcal{N}}$ values reported here deviates only slightly from a lognormal distribution (skewness ~0.4, kurtosis ~2.4) when excluding the top and bottom 5% quantiles to remove outliers. We therefore report $F_{\mathcal{N}}$ as the median of 1000 bootstrap iterations evaluated using a lognormal estimator (excluding eight outliers), and the associated 95% confidence interval in brackets. Pooled $F_{\mathcal{N}}$ values have a median value of 0.4 (0.3, 0.5) mmol m^{-2} d^{-1}. When calculated separately for ice-covered and open-water stations, the median values are 0.3 (0.2, 0.4) mmol m^{-2} d^{-1} and 0.7 (0.4, 1.1) mmol m^{-2} d^{-1}, respectively (see Figure 7 and Table 1).

3.3. New and Regenerated Production

Nitrate uptake determined from the incubations (integrated from the surface to halfway into the nitracline) for the May stations (P1-4) range from 2.6 to 8.4 mmol m^{-2} d^{-1}, while August stations (P5-P7) range from 0.015 to 0.048 mmol m^{-2} d^{-1} (see Tab. 2). Taking into account interpolation errors and the slight arbitrariness of the lower integration depth (± 5 m), we estimate a statistical uncertainty of approximately 10% in the uptake rates. $F_{\mathcal{N}}$ was smaller than NO_3^- uptake at the May stations, while at the August stations, $F_{\mathcal{N}}$ was more than an order of magnitude larger than uptake.

4. Discussion

4.1. Interpreting Nitrate Fluxes

Calculation and interpretation of the nitrate fluxes are hampered by (1) frequently shallow (<15 m) and complex pycnocline and nitracline structures, and (2) the frequently deeper vertical position of the nitracline relative to the pycnocline (Figure 6). (1) leads to a large degree of intermittency due to the proximity to wind forcing at the ocean surface. (2) Can be due to assimilation of nitrate under the pycnocline when the pycnocline is shallower than the euphotic zone, or because of continued ice melt which can shoal the seasonal pycnocline after the establishment of the nitracline. Therefore, although the pycnocline often presents the "bottleneck" in the upward transport of tracers due to its strong stratification, its effect on $F_{\mathcal{N}}$ in many cases is to isolate the nitracline from dissipation of wind energy [cf. *Randelhoff et al.*, 2014].

In the study area, advection of nutrients with the inflow of Atlantic Water is potentially an important process. Similarly, previous studies have pointed at the importance of eddies for the cross-slope transport of nutrients and biomass into the deep Arctic basin [e.g., *Watanabe et al.*, 2014]. Findings by *Hattermann et al.* [2016]

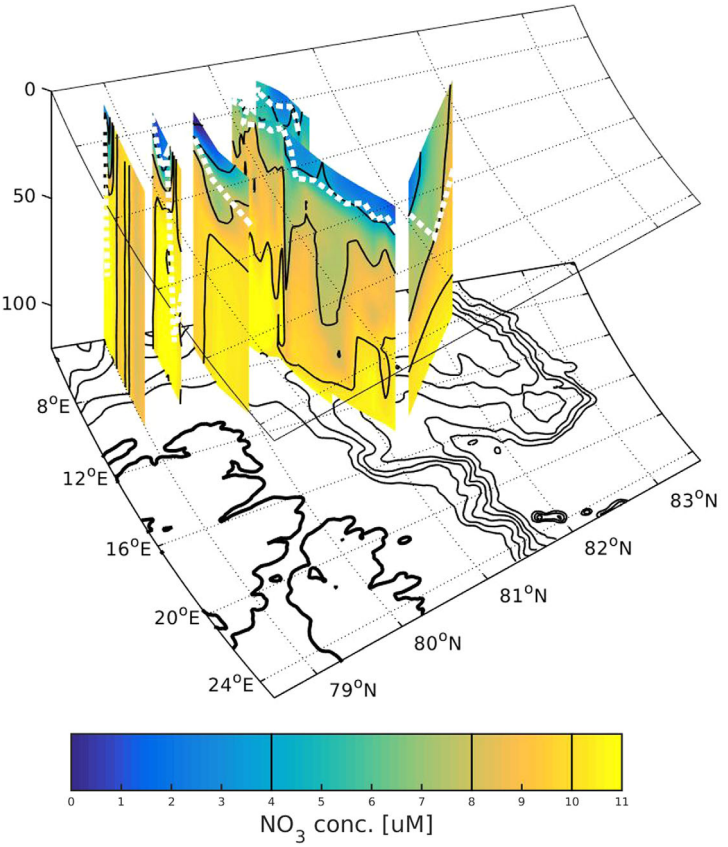

Figure 3. Curtain plots of nitrate concentration $\mathcal{N}$: Spring (N-ICE from 27 May, CarbonBridge May data, TRANSSIZ). Mixed layer depth is plotted into the curtains as dotted lines.

indicate that the Sofia Deep (the region between the Yermak Plateau and the shelf slope) does not have much eddy activity, but the western flank of the Yermak plateau does. In early spring, when differences in bloom timing lead to horizontal gradients, horizontal transport with eddies or the Atlantic Water can lead to a wide redistribution of nutrients. As the season progresses, however, surface waters become similarly depleted across the study area (Figure 4), decreasing the importance of horizontal transport. As we will show shortly, our measurements of the nitrate uptake rates do not indicate any additional supply of nitrate in late summer.

Upwelling, i.e., wind induced Ekman pumping, may lift the nitracline and bring nutrients closer to the surface. If this occurs in the summer season, local production may be temporarily increased by exposing more nitrate to sufficient radiation. However, analysis of wind curl over multiple years [*Lind and Ingvaldsen*, 2012] indicates that Ekman pumping in this area is substantially weaker in summer than in winter, when it would facilitate redistribution of nutrients in the water column rather than contribute directly to increased primary production. In slope areas where there currently is not enough vertical redistribution of nutrients to replenish the upper column in winter, enhanced upwelling may increase overall productivity. However, since the water column in the Svalbard shelf slope area is already well-mixed through large parts of the winter [see also *Randelhoff et al.*, 2015], winter upwelling does not increase productivity in this area. Furthermore, the large increases in upwelling seen on the Canadian shelf [e.g., *Tremblay et al.*, 2015] are also contingent on the dominant wind direction being east.

4.2. Magnitude and Spatial Patterns in Fluxes

Subsampling by season and presence of ice cover shows that the presence of ice cover has a larger influence on the magnitude of $F_{\mathcal{N}}$ (cf. Table 1) than the season. This means the seasonal variability is small as long as the ice concentrations are similar; however, the fluxes in open waters are generally larger. In August, nitraclines are deeper and less stratified, and the surface waters are more nutrient-depleted. Note that the weaker stratification in August is mostly due to the migration of the nitracline below the seasonal pycnocline. The small sample size (n = 2, out of seven relevant ISUS profiles with colocated MSS measurements) of open-water $F_{\mathcal{N}}$ in May demonstrates that most of the profiles do not show a sufficient amount of nitrate drawdown and hence no nitracline. Given the comparable vertical nitrate gradients in all subsamples, the consistently weaker stratification seems to be the main cause for the enhanced fluxes in open water since dissipation values show at most a small increase. Open water may allow for additional mixing processes at the surface such as gravity waves, Langmuir turbulence or enhanced input of near-inertial wind energy; however, no conclusive answer can be reached based on this data set. Most of the other external parameters relevant for mixing processes (e.g., bottom depth, tidal, and boundary current intensities, ice cover,

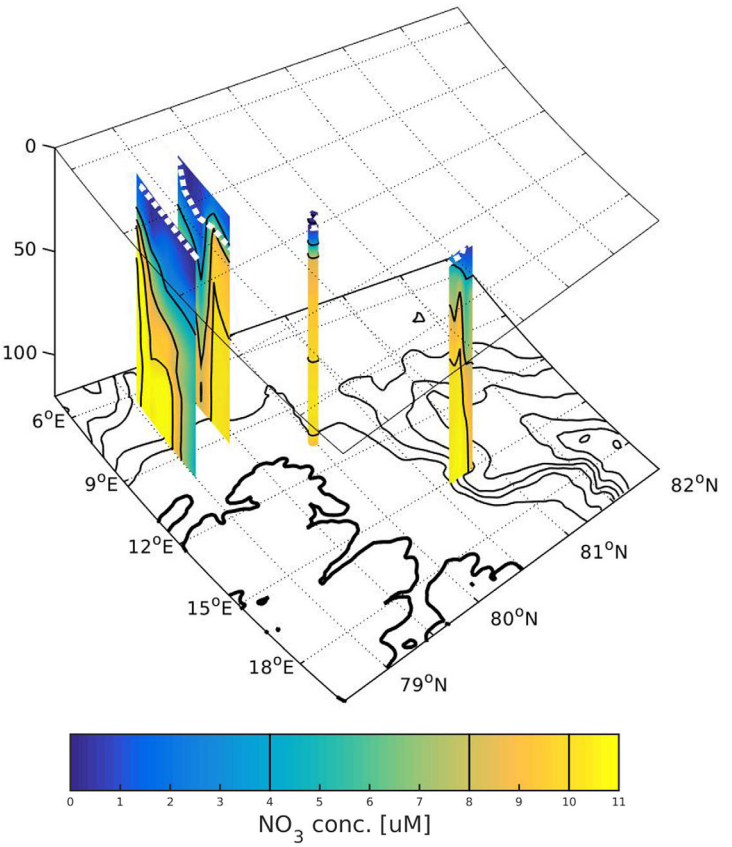

Figure 4. Curtain plots of nitrate concentration $\mathcal{N}$: Summer (CarbonBridge August data). Mixed layer depth is plotted into the curtains as dotted lines.

surface stratification) largely covary with one another in this region, and attempts at separating their relative contributions have not proved fruitful in the present data set.

A frequent caveat in previous studies on turbulent nitrate fluxes in the Arctic is the small number of observations which makes the analysis prone to outliers, and renders deriving long-term averages speculative. *Sundfjord et al.* [2007] find 0.14 mmol m^{-2} d^{-1} for a rather quiescent station in the Northern Barents Sea, and contrast this with a much higher flux of 2.4 mmol m^{-2} d^{-1} at a nearby station subject to strong tidal mixing. Since these values bracket our estimates generously, we argue that they do not represent long-term or large-scale averages but might be indicative of relative geographical trends, and govern local biological processes on shorter time scales. The same is probably

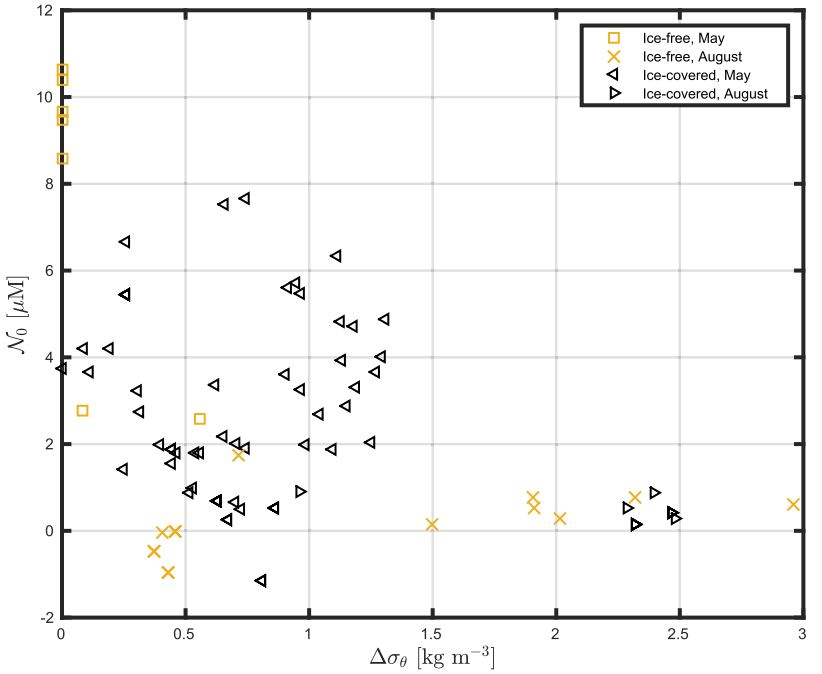

Figure 5. Surface nitrate concentration $\mathcal{N}_0$ plotted against the difference in potential density ($\Delta\sigma_\theta$) between surface and "deep" (50–60 m) water.

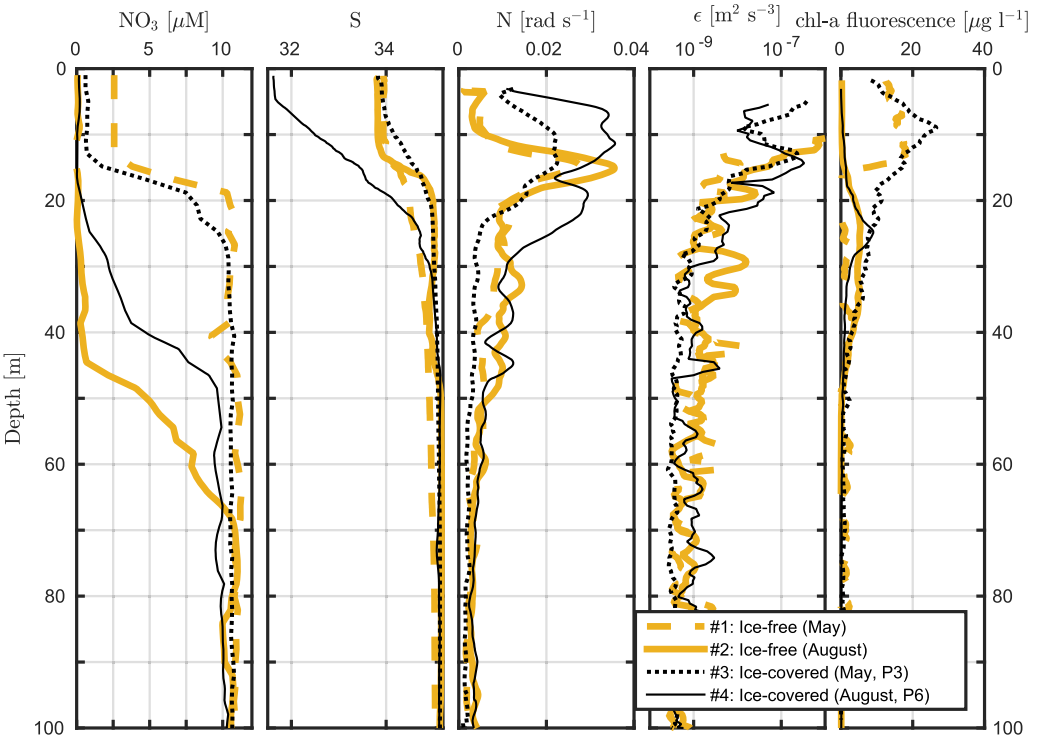

Figure 6. Four vertical profiles of NO_3^- concentration, salinity, buoyancy frequency, dissipation rate, and chl-a fluorescence highlighting aspects of the seasonality of primary productivity in the Arctic (#1, May, and #2, August: Open water, approximately 79° N, 5° E. #3: P3, #4: P6, both ice-covered, see also Figure 1). Chl-a fluorescence is uncalibrated, reported as measured by a Turner Cyclops-7 fluorometer mounted on the MSS. Note that the upper ~10 m of dissipation profiles sampled from the vessel are excluded.

true for two other estimates in the Barents Sea ($F_{\mathcal{N}} \sim 0.05$ mmol m^{-2} d^{-1} and ~2 mmol m^{-2} d^{-1}, I. Wiedmann, personal communication, 2015), contrasting two different stratification regimes north and south of the Polar Front, respectively. *Bourgault et al.* [2011] estimate autumn $F_{\mathcal{N}}$ in the ice-covered southeast

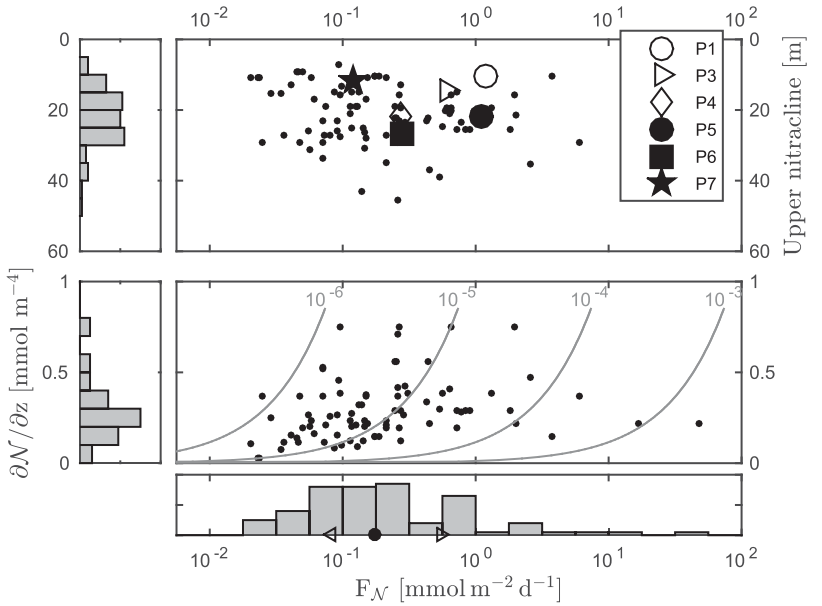

Figure 7. Histogram of nitrate fluxes. Black dot and triangles in the lower plot indicate median and 25% and 75% percentiles, respectively (see text). The grey contour lines indicate eddy diffusivity (units m^2 s^{-1}). "Upper nitracline" is the upper extent of the nitracline as determined by the algorithm described in Appendix B.

Table 1. Average Values of Selected Parameters Binned According to Ice Cover and Season[a]

	Ice Covered		No Ice	
	May	August	May	August
$F_{\mathcal{N}}$ (mmol m^{-2} d^{-1})	0.3 (0.2, 0.5)	0.2 (0.1, 0.9)	0.4	0.7 (0.4, 1.3)
ϵ ($10^{-9} \cdot m^2$ s^{-3})	8.1 (6.3,14)	8.1 (3.4, 56)	2.8	11 (6.6, 26)
$\frac{\partial \mathcal{N}}{\partial z}$ (μM m^{-1})	0.2 (0.2, 0.4)	0.3 (0.2, 0.4)	0.32	0.3 (0.2, 0.5)
N^2 ($10^{-4} \cdot s^{-2}$)	2.0 (1.1, 3.1)	1.2 (1.0, 2.2)	0.5	0.9 (0.8, 1.2)
Δz (m)	4 (1, 8)	16 (13, 18)	0	13 (8, 17)
NO_3^- surface conc. (μM)	2 (0.8, 4.2)	0.4 (0.2, 0.5)	2.7	0.02
Sample size, n	56	12	2	18

[a]The sample size is the number of valid $F_{\mathcal{N}}$ estimates; the number of profiles might be larger (see text). "Averages" are either the median of the lognormal estimator used on 1000 bootstrap iterations ($F_{\mathcal{N}}$: vertical nitrate flux, ϵ: dissipation rate of turbulent kinetic energy in the nitracline) or the median values of all samples in the respective category for that parameter ($\frac{\partial \mathcal{N}}{\partial z}$: nitrate concentration gradient across nitracline, N^2: buoyancy frequency squared across nitracline, Δz: difference between the upper extents of the nitracline and the pycnocline (positive: nitracline deeper than pycnocline), NO_3^- surface concentration). In brackets, the 95% bootstrapped confidence interval or the first and third quartiles are given, respectively. For the two open-water profiles in May, just the mean values are given.

Beaufort Sea, and find a flux of 0.5 mmol m^{-2} d^{-1}, which is about twice as large as our estimate for $F_{\mathcal{N}}$ under ice-covered conditions. The season and regional hydrography are somewhat different and so the flux magnitudes compare reasonably well.

The vertical mixing that (together with remineralization) is responsible for restoring the prebloom nitrate pool during winter has been estimated to be slightly less than 2.5 mmol m^{-2} d^{-1} in the AW inflow [*Randelhoff et al*., 2015], likely aided by thermal convection and therefore reasonably high compared to our value. In addition, *Nishino et al*. [2015] found an upward nitrate flux of 3.5 mmol m^{-2} d^{-1} at the base of the mixed layer following several strong wind events in the northern Chukchi Sea in autumn, similarly suggesting that fall mixing might be stronger than the rather small values reported in the present study. Indeed, *Ardyna et al*. [2014] report an increase in the number of secondary late-autumn blooms which could also contribute to annual new production as a consequence of enhanced upward mixing of nitrate while there is still sufficient light. Our August cruise was probably too early to pick up any such bloom, but to our knowledge, they have so far not been investigated in the field in this area.

The data set presented in this paper covers a wide range of seasons, locations, and types of ice cover, with a large number of $F_{\mathcal{N}}$ estimates. We therefore expect that the statistics are robust and our data set can be used to constrain both observations of Arctic primary production and biogeochemical ocean circulation models.

4.3. Nitrate Uptake Rates

The fact that during May, $F_{\mathcal{N}}$ was smaller than NO_3^- uptake is consistent with the stipulation that early in the season surface $\mathcal{N}$ is large enough that it is not limiting new production, even when it is certainly approaching depletion. In addition, the nitracline is sufficiently shallow in May that nitrate demand can be

Table 2. Overview Over $F_{\mathcal{N}}$ (NO_3^- Fluxes) (Given as Bootstrap Using a Lognormal Estimator and 95% Confidence Interval in Brackets), Consumption of NO_3^- ($\int dz\, NO_3^-$ upt.) and NH_4^+ ($\int dz\, NH_4^+$ upt.) (Both (mmol m^{-2} d^{-1})), and Surface Concentrations (μM) of NO_3^- and NH_4^+ at the CarbonBridge Process Stations[a]

	$F_{\mathcal{N}}$	$\int dz\, NO_3^-$ upt.	$\int dz\, NH_4^+$ upt.	NO_3^- sfc. conc.	NH_4^+ sfc. conc.
P1	1.2 (0.2, 5.6)	2.6	1.1	2.5	0.07
P3	0.6 (0.2, 2)	3.1	5.3	0.44	0.17
P4	0.3 (0.2, 0.3)	8.4	4.8	0.33	0.05
P5	1.1 (0.7, 1.7)[b]	0.015	5.8	0.11	0.15
P6	0.3 (0.1, 0.8)	0.018	2.3	0.07	0.08
P7	0.1[c]	0.048	2.1	0.26	0.02

[a]P1-4 were conducted in May, P5-7 in August. For station locations, see Figure 1. P1 and P5 are approximately colocated. Uptake rates are integrated from the surface to halfway into the nitracline.

[b]This is after excluding the top and bottom 5% of the distribution to remove the outliers (as described in the text), all of which are located on P5. Not removing these results in an estimate 5.9 (1.5, 47) mmol m^{-2} d^{-1}, but it is difficult to assess the relative contribution of these high-mixing events due to the small sample number (n = 11 nitrate flux estimates).

[c]n = 1.

fulfilled by a net downward displacement of the standing stock, which then relies on ambient nitrate inventories to a greater extent than on $F_{\mathcal{N}}$.

Since August nutrient concentrations were extremely small, one would expect that the uptake of nitrate were bounded by its supply through vertical fluxes. However, our measurements suggest that the nitrate supplied through vertical mixing actually exceeded its uptake by a factor of more than 10. Smaller flagellates dominated the microalgal community in August. Thus although the low silicate concentration $<2\ \mu M$ (data not shown) likely inhibited growth of diatoms, it was not a limiting factor for nitrate uptake. Several other possibilities exist to explain the large discrepancy between measured values of $F_{\mathcal{N}}$ and NO_3^- uptake in August. If the measurements were to be inaccurate, the discrepancy could be either due to an overestimation of $F_{\mathcal{N}}$ or an underestimation of NO_3^- uptake. It seems implausible that the mixing efficiency used in the estimation of the eddy diffusivity would be consistently that much smaller than the value of 0.2 we used in this study (see section 2.2). At low $\mathcal{N}$, one might think that NO_3^- uptake during the incubation will make NO_3^- limitation even stronger, but the measured uptake rate is still orders of magnitude far from depleting the nitrate pool during the 24 h incubation period.

The lack of turbulence in the incubation bottles might artificially reduce the uptake rate. Indeed, *Aksnes and Egge* [1991] argue for an extension of NO_3^- uptake Michaelis-Menten kinetics that includes a toward-cell diffusive transport coefficient. At low nutrient concentrations, this implies a linear dependence on turbulent shear levels, which might account for the order-of-magnitude discrepancy between inside-bottle and hypothetical outside-bottle uptake rates.

It is worth noting that NH_4^+ uptake rates were two orders of magnitude higher than NO_3^- uptake rates at the surface of stations P5 and P6 (not shown but see Table 2 for integrated rates), despite the evenness of incubation conditions and ambient concentrations for the two nitrogen sources. This pattern suggests a strong preference of the community for reduced nitrogen and/or intense recycling within the incubation bottles. Under strong recycling, the nitrogen initially taken up as nitrate may not accumulate in phytoplankton biomass, either supporting a fast turnover of NH_4^+ or a transient build-up of dissolved organic pools (not measured here). In addition, previous studies have shown that net nitrate uptake (i.e., the accumulation of N in particulate matter) by phytoplankton may represent as little as 26% of gross nitrate uptake [*Bronk and Ward*, 2000], but this was not assessed here. In the case of preference, the upward supply of nitrate would lead to a progressive accumulation of NO_3^- into the euphotic zone, but this cannot be confirmed in the absence of Lagrangian sampling. Furthermore, the increase would be hardly noticeable over the involved timescales (for instance, a surplus of 0.5 mmol m^{-2} d^{-1} distributed over 20 m depth corresponds to an increase of 0.75 μM $month^{-1}$).

If the inside-bottle uptake rates are indeed representative of the "real" uptake rates outside the bottles even in August, we will have to revise our hypothesis that new production is limited by NO_3^- availability. However, we have not found a compelling explanation for this scenario.

4.4. New Production

To put our flux estimates into context, assuming a Redfield C:N ratio of 106:16, $F_{\mathcal{N}} \approx 0.3$mmol m^{-2} d^{-1} would correspond to a new production of $\sim$0.7 g C m^{-2} $month^{-1}$, amounting to approximately 3 g C m^{-2} during the summer season. Compared to nitrate-based estimates of yearly new production of around 47 g C m^{-2} (Barents Sea shelf), 31 g C m^{-2} (shelf slope) and 13 g C m^{-2} (Eurasian Basin) [*Codispoti et al*., 2013; *Randelhoff et al*., 2015], the vertical flux during summer only plays a small role in determining the annual nitrate drawdown on the productive shelves, and that (a) preconditioning (filling up the prebloom reservoir of nitrate) and (b) the development of a subsurface chlorophyll maximum account for most of the annual nitrate drawdown. Thus the increase in net primary production in the Barents Sea reported by *Arrigo and van Dijken* [2015] might represent mostly an increase in regenerated production, not supporting additional carbon export. The new production in summer might, however, represent a significant fraction of the annual nitrate drawdown in the Eurasian Basin and thus exert an important control on the export production there, including the modification of geochemical nutrient and carbon cycles. Strengthening of the perennial, deep stratification (for instance, between AW and the Polar Mixed Layer in the Eurasian Basin) by changing freshwater budgets [see e.g., *Nummelin et al*., 2015] is an altogether different issue and only marginally related to seasonal sea ice melt, and left to further studies.

At any rate, it can be expected that the magnitude of $F_{\mathcal{N}}$ will determine the extent to which a community enters a recycling (NH_4^+ -dependent) state postbloom, or that a smaller $F_{\mathcal{N}}$ favors smaller phytoplankton with higher affinity for reduced nitrogen resources [e.g., *Li et al*., 2009; *Sommer et al*., 2016]. This is also reflected in our observations: the phytoplankton community in May/June was dominated by a combination of both the haptophyte *Phaeocystis pouchetii* and larger diatoms (Carbon Bridge May cruise), or completely by *P. pouchetii* (N-ICE; P. Assmy, personal communication, 2016). In August, however, smaller flagellates dominated the phytoplankton community, probably in response to low nutrient concentrations. The relatively low values of $F_{\mathcal{N}}$ are therefore important because they help to produce these oligotrophic conditions.

5. Summary and Perspectives

Based on this study, we draw the following conclusions: (a) close to the shelf, upper ocean $\mathcal{N}$ is homogeneous with depth at approximately 10 μM, from early winter until the bloom starts. In the deep basin, permanent nitrate stratification exists also prebloom (albeit across a deep pycnocline), with surface mixed layer $\mathcal{N}$ as low as approximately 5 μM. (b) The $\mathcal{N}$ drawdown in the photic zone is empirically strongly related to the development of seasonal stratification from ice melt. This agrees with Sverdrup's critical mixing theory [*Sverdrup*, 1953] and is presumably related to reduction in eddy diffusivity with increasing stratification, which increases residence time of individual phytoplankton cells in the low-light photic zone of the Arctic Ocean. (c) Upward turbulent nitrate fluxes across the seasonal nitracline in the study area are small ($\sim$0.3 mmol m^{-2} d^{-1} in ice-covered areas, and about twice as much in ice-free conditions) compared to overall estimates of annual NO_3^- drawdown.

Comparison with estimates of late summer NO_3^- uptake was inconclusive. We have not found a compelling explanation for what else might have limited NO_3^- accumulation in particulate matter by an order of magnitude more than $F_{\mathcal{N}}$, and it is possible that the bottle incubation technique underestimated NO_3^- uptake. However, we observed a strong uptake preference for NH_4^+, and the corresponding increase in $\mathcal{N}$ would be small and hard to detect even with dedicated sampling schemes.

On a pan-Arctic scale, the near-surface warm AW inflow along the shelf slope is a regional anomaly. In the context of this study, AW heat leads to stronger melt rates [*Onarheim et al*., 2014] and therefore earlier onset of stratification and might thus be indirectly linked to bloom development (cf. point (b) above). However, we expect that much of the seasonal upper ocean hydrography and accordingly nitrate fluxes are governed by similar mechanisms across the ice-covered Arctic, with local adjustments for different melt rates, thus vertical density gradients, and different nitrate concentration gradients.

The vertical nitrate fluxes presented here could entail an increase in new production of a few g C m^{-2} under the transition to a seasonal ice cover, with ensuing changes in boundary layer stratification being the biggest driver. This would be a significant fraction of the current export production in the deep Eurasian Basin, but hardly noticeable on the productive shelves.

Appendix A: ISUS Data Processing and Quality Control

Some ISUS profiles show clear signs of "nitrate spiking" when the CTD traverses a halo or thermocline (akin to salinity spiking known from standard CTD processing procedures), indicating (1) some degree of misalignment between ISUS and T-S records, and (2) low-pass effects stemming from using the ISUS in an unpumped configuration. While these features could be somewhat relieved by adjusting the ISUS lag for individual casts (introduced to account for the combined effect of differing heights of the sensors on the instrument package and the T-S package being pumped), finding objective criteria proved difficult, presumably among other things due to different horizontal velocities of the instrument package relative to the surrounding water, leading to variable turnover times of the water parcel in the sensor tip. However, averaging vertically in 2 m bins, bulk $\mathcal{N}$ gradients in the nitracline are found to be virtually independent of the specific choice of the time lag within a few seconds.

Most often, a depth-independent bias in computed $\mathcal{N}$ was detected from comparison with bottle samples taken during the same CTD casts during the CarbonBridge campaigns, the ISUS being biased high by about 0 to 2μM on a per-campaign basis (cf. Figure 8). Each profile was then adjusted by subtracting a

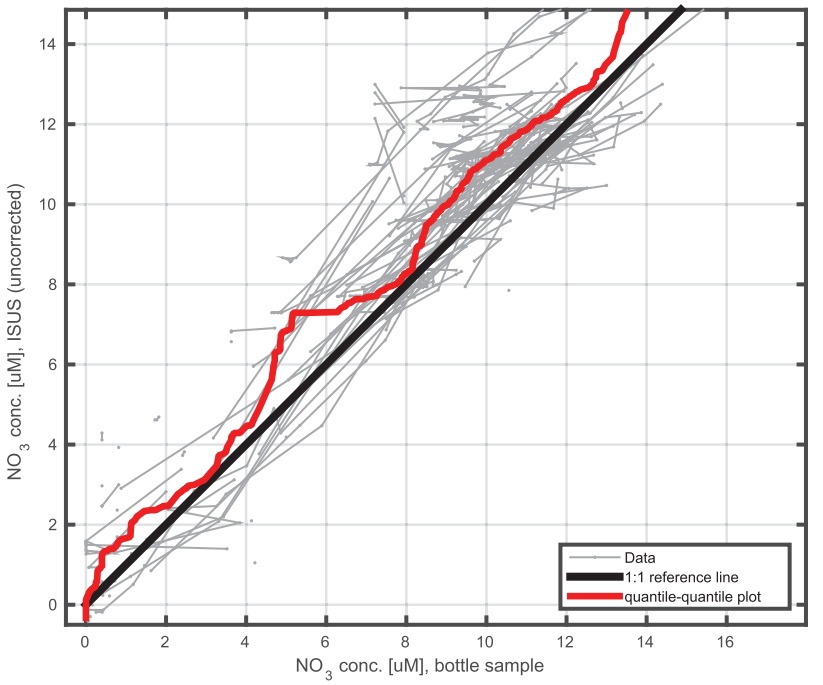

Figure 8. $\mathcal{N}$ from ISUS versus bottle samples. Individual profiles are connected by thin lines. Note that these ISUS concentration values are not corrected against bottle samples.

constant offset, determined for each profile individually as the average offset between bottle samples and ISUS.

For the N-ICE campaign, bottle samples were generally farther removed from ISUS profiles, both in time and accordingly in space. For all profiles, manually selected bottle sample profiles sufficiently close in space, T-S properties, and vertical $\mathcal{N}$ structure were compared to judge and correct for a depth-independent bias. In some instances, profiles lacking good quality data in the uppermost few tens of meters (presumably due to either turbid waters or instrument lamp warmup issues) were extrapolated using the bottle profile given that these were sufficiently close in T-S properties.

Quantiles of profile-wise RMSEs between ISUS and bottle samples were 0.4, 0.9, 1.2, and 3.5 μM (in this order: median corrected and uncorrected and 95% quantile corrected and uncorrected). A quantile-quantile plot (see Figure 8) further demonstrates that the ISUS has a tendency to overestimate bottle $\mathcal{N}$ (slight offset above the 1:1 reference line), but importantly no systematic deviation from a linear response (as indicated by the 1:1 slope).

Final profiles of $\mathcal{N}$ were produced at 2 m resolution. The resulting $\mathcal{N}$ profiles from all campaigns were visually quality-controlled.

Appendix B: Nitracline Detection and Estimation of the Vertical Turbulent Nitrate Flux

The nitracline is defined as the depth interval where $\mathcal{N}$ crosses from 20% to 80% of the $\mathcal{N}$ difference between the surface value (calculated across 3–8 m) and a "deep" reference value (calculated across 50–60 m). The 50–60 m depth interval was selected after inspection of all potential density (σ_θ) profiles included in this study. The pycnocline is defined similarly for σ_θ, except, in order to account for the strong near-surface stratification, the surface value is calculated as the average between 3 m and the depth where the buoyancy frequency N exceeds $2{\cdot}10^{-3}$ s^{-1} for the first time. A density-scaled depth coordinate $r_\sigma = (\sigma_\theta(z) - \sigma_\theta(\mathrm{sfc}))/\Delta\sigma_\theta$ is introduced which corresponds to how much of the density difference $\Delta\sigma_\theta$ between "surface" and "deep" value the density profile has crossed, such that it is always 0 in the surface and 1 below 60 m. $\frac{\partial \mathcal{N}}{\partial z}$ is the slope of the linear regression of $\mathcal{N}$ against depth over the nitracline. For an individual profile, K_ρ is calculated as $0.2\epsilon/N^2$, where ϵ

is the mean of all dissipation values across the nitracline for a given profile, and the buoyancy frequency N is calculated using the density gradient obtained from a least-squares regression of σ_θ against depth for each profile. To ensure that variations in depths of isopycnals between individual profiles do not disturb the averages by including elevated near-surface values of K_ρ, the nitracline is expressed as an interval of r_σ (based on the density profile associated with the CTD+ISUS cast), and the nitracline in an MSS profile is defined as the same r_σ interval, based on the σ_θ profile associated with the MSS cast. This definition of isopycnals ensures that drift in the conductivity cells does not lead to a bias in the densities and thus to artificial isopycnal excursions. Since surface layer values are calculated between 3 and 8 m depth, we do not expect ship-based CTD salinities to be significantly biased high due to ship disturbance, relative to ice-floe-based MSS profiles.

Acknowledgments

CarbonBridge data collection and A.R.'s work was supported through the project CARBON BRIDGE: Bridging marine productivity regimes: How Atlantic advective inflow affects productivity, carbon cycling, and export in a melting Arctic Ocean, a Polar Programme (project 226415) funded by the Norwegian Research Council. N-ICE data collection was supported by the Norwegian Polar Institutes Centre for Ice, Climate and Ecosystems (ICE) through the N-ICE project, with additional support from the Ministry of Climate and Environment, and Ministry of Foreign Affairs of Norway. The ISUS deployments from R/V Polarstern were conducted during the ARKXXIX/1-PS92 TRANSSIZ cruise (Transitions in the Arctic Seasonal Sea Ice Zone), grant no. AWI_PS92_00. We thank the captains and crews of R/Vs Helmer Hanssen, Lance and Polarstern, and all the scientists involved in the field campaigns for their support. Svein Kristiansen analyzed the nitrate samples for the CarbonBridge and TransSIZ campaigns. We thank two anonymous reviewers for their comments. The data published in this article will be made accessible through the Norwegian Polar Data Centre (data.npolar.no) and the Norwegian Marine Data Centre (www.nmdc.no).

References

Aksnes, D., and J. Egge (1991), A theoretical model for nutrient uptake in phytoplankton, *Mar. Ecol. Prog. Ser.*, *70*(1), 65–72.

Ardyna, M., M. Babin, M. Gosselin, E. Devred, L. Rainville, and J.-E. Tremblay (2014), Recent Arctic Ocean sea ice loss triggers novel fall phytoplankton blooms, *Geophys. Res. Lett.*, *41*, 6207–6212, doi:10.1002/2014GL061047.

Arrigo, K. R., and G. L. van Dijken (2015), Continued increases in Arctic Ocean primary production, *Prog. Oceanogr.*, *136*, 60–70, doi:10.1016/j.pocean.2015.05.002.

Bendschneider, K., and R. Robinson (1952), A new spectrophotometric method for the determination of nitrite in sea water, *J. Mar. Res.*, *11*, 87–96.

Blais, M., J.-E. Tremblay, A. D. Jungblut, J. Gagnon, J. Martin, M. Thaler, and C. Lovejoy (2012), Nitrogen fixation and identification of potential diazotrophs in the Canadian Arctic, *Global Biogeochem. Cycles*, *26*, GB3022, doi:10.1029/2011GB004096.

Bourgault, D., C. Hamel, F. Cyr, J.-E. Tremblay, P. S. Galbraith, D. Dumont, and Y. Gratton (2011), Turbulent nitrate fluxes in the Amundsen Gulf during ice-covered conditions, *Geophys. Res. Lett.*, *38*, L15602, doi:10.1029/2011GL047936.

Bronk, D. A., and B. B. Ward (2000), Magnitude of dissolved organic nitrogen release relative to gross nitrogen uptake in marine systems, *Limnol. Oceanogr.*, *45*(8), 1879–1883, doi:10.4319/lo.2000.45.8.1879.

Codispoti, L., V. Kelly, A. Thessen, P. Matrai, S. Suttles, V. Hill, M. Steele, and B. Light (2013), Synthesis of primary production in the Arctic Ocean: III. Nitrate and phosphate based estimates of net community production, *Prog. Oceanogr.*, *110*, 126–150, doi:10.1016/j.pocean.2012.11.006.

Collos, Y. (1987), Calculations of 15N uptake rates by phytoplankton assimilating one or several nitrogen sources, *Int. J. Rad. Appl. Instrum. A*, *38*(4), 275–282, doi:10.1016/0883-2889(87)90038-4.

Dugdale, R. C., and J. J. Goering (1967), Uptake of new and regenerated forms of nitrogen in primary productivity, *Limnol. Oceanogr.*, *12*(2), 196–206, doi:10.4319/lo.1967.12.2. 0196.

Eppley, R., and B. Peterson (1979), The flux of particulate organic matter to the deep ocean and its relation to planktonic new production, *Nature*, *282*, 677–680.

Fer, I. (2006), Scaling turbulent dissipation in an Arctic fjord, *Deep Sea Res., Part II*, *53*, 77–95, doi:10.1016/j.dsr2.2006.01.003.

Granskog, M., P. Assmy, S. Gerland, G. Spreen, H. Steen, and L. Smedsrud (2016), Arctic research on thin ice: Consequences of Arctic sea ice loss, *Eos Trans. AGU*, *97*, doi:10.1029/2016eo044097.

Hattermann, T., P. E. Isachsen, W.-J. von Appen, J. Albretsen, and A. Sundfjord (2016), Eddy-driven recirculation of Atlantic water in Fram Strait, *Geophys. Res. Lett.*, *43*, 3406–3414, doi:10.1002/2016GL068323.

Holmes, R. M., A. Aminot, R. Kérouel, B. A. Hooker, and B. J. Peterson (1999), A simple and precise method for measuring ammonium in marine and freshwater ecosystems, *Can. J. Fish. Aquat. Sci.*, *56*(10), 1801–1808, doi:10.1139/f99-128.

Jakobsson, M., et al. (2012), The International Bathymetric Chart of the Arctic Ocean (IBCAO) Version 3.0, *Geophys. Res. Lett.*, *39*, L12609, doi:10.1029/2012GL052219.

Li, W. K. W., F. A. McLaughlin, C. Lovejoy, and E. C. Carmack (2009), Smallest algae thrive as the Arctic Ocean freshens, *Science*, *326*(5952), 539–539, doi:10.1126/science.1179798.

Lind, S., and R. B. Ingvaldsen (2012), Variability and impacts of Atlantic Water entering the Barents Sea from the north, *Deep Sea Res., Part I*, *62*, 70–88, doi:10.1016/j.dsr.2011.12.007.

Nishino, S., Y. Kawaguchi, J. Inoue, T. Hirawake, A. Fujiwara, R. Futsuki, J. Onodera, and M. Aoyama (2015), Nutrient supply and biological response to wind-induced mixing, inertial motion, internal waves, and currents in the northern Chukchi Sea, *J. Geophys. Res. Oceans*, *120*, 1975–1992, doi:10.1002/2014JC010407.

Nummelin, A., M. Ilicak, C. Li, and L. H. Smedsrud (2015), Consequences of future increased Arctic runoff on Arctic Ocean stratification, circulation, and sea ice cover, *J. Geophys. Res. Oceans*, *121*, 617–637, doi:10.1002/2015JC011156.

Onarheim, I. H., L. H. Smedsrud, R. B. Ingvaldsen, and F. Nilsen (2014), Loss of sea ice during winter north of svalbard, *Tellus Ser. A*, *66*, doi:10.3402/tellusa.v66.23933.

Osborn, T. R. (1980), Estimates of the local rate of vertical diffusion from dissipation measurements, *J. Phys. Oceanogr.*, *10*(1), 83–89, doi:10.1175/1520-0485(1980)010 < 0083:EOTLRO>2.0.CO;2.

Randelhoff, A., A. Sundfjord, and A. H. H. Renner (2014), Effects of a shallow pycnocline and surface meltwater on sea ice-ocean drag and turbulent heat flux, *J. Phys. Oceanogr.*, *44*(8), 2176–2190, doi:10.1175/jpo-d-13-0231.1.

Randelhoff, A., A. Sundfjord, and M. Reigstad (2015), Seasonal variability and fluxes of nitrate in the surface waters over the Arctic shelf slope, *Geophys. Res. Lett.*, *42*, 3442–3449, doi:10.1002/2015GL063655.

Sakamoto, C. M., K. S. Johnson, and L. J. Coletti (2009), Improved algorithm for the computation of nitrate concentrations in seawater using an in situ ultraviolet spectrophotometer, *Limnol. Oceanogr. Methods*, *7*, 132–143.

Sommer, U., K. H. Peter, S. Genitsaris, and M. Moustaka-Gouni (2016), Do marine phytoplankton follow Bergmanns rule sensu lato?, *Biol. Rev.*, doi:10.1111/brv.12266, in press.

Stroeve, J. C., M. C. Serreze, M. M. Holland, J. E. Kay, J. Malanik, and A. P. Barrett (2011), The Arctics rapidly shrinking sea ice cover: A research synthesis, *Clim. Change*, *110*(3-4), 1005–1027, doi:10.1007/s10584-011-0101-1.

Sundfjord, A., I. Fer, Y. Kasajima, and H. Svendsen (2007), Observations of turbulent mixing and hydrography in the marginal ice zone of the Barents Sea, *J. Geophys. Res.*, *112*, C05008, doi:10.1029/2006JC003524.

Sverdrup, H. (1953), On conditions for the vernal blooming of phytoplankton, *ICES J. Mar. Sci.*, *18*(3), 287–295.

Torres-Valdés, S., T. Tsubouchi, S. Bacon, A. C. Naveira-Garabato, R. Sanders, F. A. McLaughlin, B. Petrie, G. Kattner, K. Azetsu-Scott, and T. E. Whitledge (2013), Export of nutrients from the Arctic Ocean, *J. Geophys. Res. Oceans*, *118*, 1625–1644, doi:10.1002/jgrc.20063.

Tremblay, J.-E., et al. (2011), Climate forcing multiplies biological productivity in the coastal Arctic Ocean, *Geophys. Res. Lett.*, *38*, L18604, doi:10.1029/2011GL048825.

Tremblay, J.-E., L. G. Anderson, P. Matrai, P. Coupel, S. Bélanger, C. Michel, and M. Reigstad (2015), Global and regional drivers of nutrient supply, primary production and CO2 drawdown in the changing Arctic Ocean, *Prog. Oceanogr.*, *139*, 171–196, doi:10.1016/j.pocean.2015.08.009.

Watanabe, E., et al. (2014), Enhanced role of eddies in the Arctic marine biological pump, *Nat. Commun.*, *5*, 3950, doi:10.1038/ncomms4950.

Yamazaki, H., and T. Osborn (1990), Dissipation estimates for stratified turbulence, *J. Geophys. Res.*, *95*(C6), 9739–9744, doi:10.1029/JC095iC06p09739.